ACS APPLIED MATERIALS & INTERFACES

www.acsami.org

Research Article

Highly Efficient Non-Nucleophilic $Mg(CF_3SO_3)_2$-Based Electrolyte for High-Power Mg/S Battery

Dan Huang,[§] Shuangshuang Tan,[§] Maosheng Li, Dandan Wang, Chunhua Han, Qinyou An,* and Liqiang Mai*

Cite This: https://dx.doi.org/10.1021/acsami.0c00196

Read Online

ACCESS | Metrics & More | Article Recommendations | Supporting Information

ABSTRACT: The application of high-energy Mg/S batteries was obstructed by the insufficiency of low-cost and non-nucleophilic electrolyte. In this work, a non-nucleophilic electrolyte was prepared by facilely dissolving $Mg(CF_3SO_3)_2$, $MgCl_2$, and $AlCl_3$ in 1,2-dimethoxyethane (DME). The equilibrium species of the MTB electrolyte mainly comprise $[Mg_2(\mu\text{-}Cl)_2(DME)_4]^{2+}$ and $[(CF_3SO_3)AlCl_3]^-$, which are generated by dehalodimerization reaction and Lewis acid−base reaction, respectively. The electrolyte exhibits a highly efficient reversible Mg deposition/dissolution, low overpotential of around 250 mV, and good oxidative stability up to 3.5 V after conditioning. The conditioning process that the active $[Mg_2(\mu\text{-}Cl)_2(DME)_4]^{2+}$ species transforms into $[Mg_3(\mu_3\text{-}Cl)(\mu_2\text{-}Cl)_2(DME)_7]^{3+}$ was demonstrated, owing to the irreversible deposition of Al^{3+} on Mg foil. More importantly, this electrolyte exhibited good compatibility and kinetics for reversible Mg/MgS_x redox, resulting in a high specific capacity of 866 mAh g^{-1} at 200 mA g^{-1} and high power density of 550 W kg^{-1}. This work offers a new direction for low-cost, non-nucleophilic electrolyte and paves the way to explore high-power Mg/S batteries.

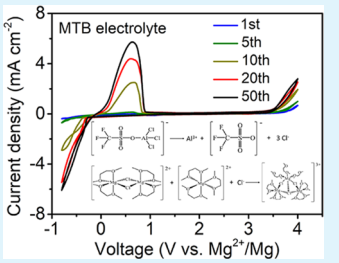

KEYWORDS: *magnesium−sulfur battery, non-nucleophilic electrolyte, high power, high efficiency, magnesium trifluoromethanesulfonate*

1. INTRODUCTION

Rechargeable lithium-ion batteries have been commercialized since the 1990s.[1] However, the growing cost and safety issues caused by lithium drastically impede their applications in large-scale storage systems. In comparison, rechargeable magnesium batteries (RMBs) have great development prospects in terms of abundant Mg resources (one of the most widely distributed elements with ∼2% in Earth's crust),[2] low cost, and high volumetric capacity (3832 mAh cm^{-3}).[3−6]

Large-scale applications of energy storage devices require high-energy-density batteries to reduce their size and mass to meet higher market demands.[7] Nevertheless, the development of high-energy-density RMBs was still hampered by the lack of compatible cathodes with high capacity, suitable electrolytes with high deposition/dissolution efficiency, high oxidative stability, and good compatibility. The sulfur cathode has gained much attention by virtue of its high theoretical capacity (1675 mAh g^{-1}).[8−11] However, the traditional nucleophilic electrolytes, such as all-phenyl complex (APC) electrolyte, are not compatible with electrophilic sulfur cathodes, thus resulting in fast capacity fading.[12] Therefore, developing non-nucleophilic Mg^{2+} ion electrolytes is indispensable for Mg/S system, where the non-nucleophilic anion species play a key role in the compatibility with a sulfur cathode.[13] Previous reports about non-nucleophilic RMBs electrolytes mainly focused on three systems: hexamethyldisilazane (HMDS)-based,[14,15] magnesium(II) bis(trifluoromethane sulfonyl) imide (Mg-$(TFSI)_2$)-based,[16,17] and boron-containing electrolytes.[18] Mg-$(HMDS)_2$-based electrolytes show good compatibility with sulfur but display inferior deposition/dissolution efficiency. $Mg(TFSI)_2$-based electrolytes have high reversibility, but poor compatibility with Mg metal restricts its applications in RMBs. In comparison, boron-containing electrolytes exhibit more comprehensive abilities, including high efficiency, low polarization, and remarkable anodic stability over 4 V. Unfortunately, the complicated preparation processes dramatically increase their cost.[19] Moreover, the high prices of $Mg(HMDS)_2$, $Mg(TFSI)_2$, and boron-containing Mg salts severely hindered their applications in Mg/S batteries for large-scale storage systems (Table S1). Besides, the slow reaction kinetics between magnesium and sulfur lead to a poor power density of Mg/S batteries.[20,21] To date, preparing a low-cost, non-nucleophilic, and high-Coulombic-efficiency electrolyte for high-power Mg/S batteries is extremely challenging.

Magnesium trifluoromethanesulfonate ($Mg(CF_3SO_3)_2$) is a reported non-nucleophilic salt that has been used in gel electrolytes due to its high ionic conductivity and stability.[22] Meanwhile, the low cost indicates that it is a potential liquid electrolyte component for Mg/S batteries.[23,24] Yang et al. were first to report that a $Mg(CF_3SO_3)_2$-based electrolyte can be applied to Mg/S batteries. However, the complex components,

Received: January 5, 2020
Accepted: March 24, 2020
Published: March 24, 2020

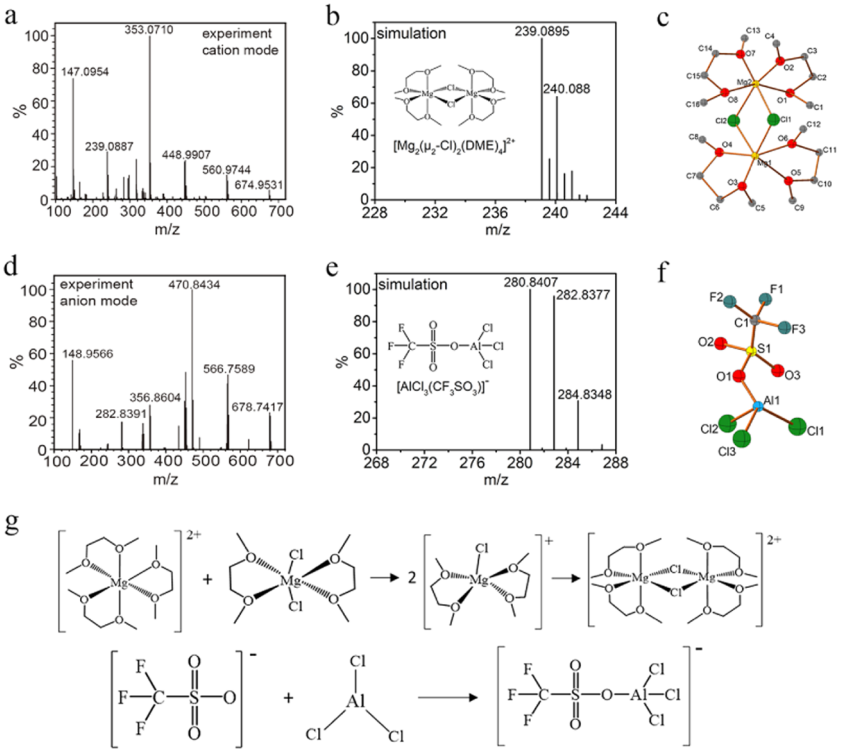

Figure 1. ESI-MS spectra of the MTB electrolyte: (a) experimental measurement and (b) simulated spectra in the positive mode and (d) experimental measurement and (e) simulated spectra in the negative mode. The molecular structure diagrams of $[Mg_2(\mu_2\text{-}Cl)_2(DME)_4]^{2+}$ (c) and $[(CF_3SO_3)AlCl_3]^-$ (f). Hydrogen atoms are omitted for clarity. (g) Possible reaction path of $Mg(CF_3SO_3)_2$ with $MgCl_2$ and $AlCl_3$ in DME solvent.

including $Mg(CF_3SO_3)_2$, $AlCl_3$, $MgCl_2$, and anthracene, in tetrahydrofuran (THF) and tetraglyme (TG) mixed solvent (1:1) increase the cost and also make the preparation more complicated. When applied in Mg/S battery, it exhibited a low specific capacity, rapid capacity fading, and high polarization.[25] This may be because the solvent and the ratio of active components are not optimized, resulting in low kinetics between reactive ionic groups and sulfur in the electrolyte.[26,27] Also, this electrolyte may not be conducive to the oxidation of the discharge product MgS. Therefore, in the $Mg(SO_3CF_3)_2$ system, the selection of a suitable solvent and the regulations to the configurations of active ions are of great significance for the electrochemical performance of Mg/S batteries.

Herein, we present a non-nucleophilic electrolyte by facilely dissolving $Mg(CF_3SO_3)_2$, $MgCl_2$, and $AlCl_3$ in 1,2-dimethoxyethane (DME). The equilibrium species of the magnesium trifluoromethanesulfonate based (MTB) electrolyte mainly comprises $[Mg_2(\mu\text{-}Cl)_2(DME)_4]^{2+}$ and $[(CF_3SO_3)AlCl_3]^-$, which are generated by dehalodimerization reaction and Lewis acid−base reaction, respectively. The cost of the MTB electrolyte is relatively low in the reported electrolytes of Mg/S batteries (Table S1). Meanwhile, the MTB electrolyte showed reversible Mg deposition/dissolution properties with high efficiency up to 99.1% after conditioning and good oxidative stability up to 3.5 V. Importantly, the conditioning process of the MTB electrolyte and the Mg^{2+} ions deposition/dissolution behavior on Mg foil in this electrolyte are explored by electron microscope and spectrum measurements. Moreover, the MTB electrolyte was successfully applied to Mg/S batteries. A high specific capacity of 866 mAh g^{-1} at 200 mA g^{-1} and 575 mAh g^{-1} at 500 mA g^{-1} are obtained. It provides a promising pathway to develop high-energy and high-power Mg/S batteries.

2. EXPERIMENTAL SECTION

2.1. Chemicals. $Mg(CF_3SO_3)_2$ (98%, Ourchem), $MgCl_2$ (99.99%, Macklin), $AlCl_3$ (99.999%, Sigma-Aldrich), DME (99.5%, Sigma-Aldrich), ammonium metavanadate (NH_4VO_3, AR, Sinopharm), hydrazine hydrate solution ($H_4N_2{\cdot}H_2O$, AR, Sinopharm), sulfur powder (S, 99.5%, Alfa Aesar), poly(vinyl difluoride) (PVDF, Xiya reagent), and *N*-methyl-2-pyrrolidinone (NMP, 98%, Aladdin).

2.2. Preparation of the MTB Electrolyte. First, 1.290 g of $Mg(CF_3SO_3)_2$ (4 mmol) was dissolved in 20 ml of DME with magnetic stirring for 2 h. Then, 0.762 g of $MgCl_2$ (8 mmol) was added into the solution and stirred for 6 h. Finally, 1.067 g of $AlCl_3$ (8 mmol) was slowly added into the above solution with magnetic stirring at 60 °C for 12 h. Excessive Mg powders were added to the final solution to remove the trace water by magnetic stirring at 40 °C for 12 h.

2.3. Synthesis of VN/60S. First, VOOH was prepared according to the previously published work.[28] Then, the VN precursor was obtained by annealing the as-prepared VOOH under NH_3 atmosphere at 550 °C for 2 h. Finally, VN/60S was prepared via a melt-diffusion strategy in which the as-prepared VN (40 g) and sulfur powder (60 g) were mixed in a mortar and heated at 160 °C for 12 h in a sealed stainless steel autoclave filled with Ar.

2.4. Preparation of Cathodes. The VN/60S cathodes were prepared by ball-milling 80 wt % VN/60S powders, 10 wt % acetylene black, and 10 wt % PVDF in NMP to obtain a homogeneous slurry, which was then pasted onto the Cu foil. The Cu foil was tailored into a proper disk with a diameter of 1 cm.

2.5. Details of Cell Assembly. Prototype rechargeable Mg batteries in coin-type cells (standard 2016 coin cell) were assembled from a fresh polished Mg disk anode, a cathode, a Mo current collector and a separator (glass fiber) soaked in the MTB electrolyte solution.

2.6. Characterization. Scanning electron microscopy (SEM) images were obtained using a JEOL-7100F microscope. Energy-dispersive spectrometer (EDS) images were obtained by a JEM-2100F-STEM/EDS microscope. X-ray diffraction (XRD) measurements were carried out by a D8 Advance X-ray diffractometer, Cu Kα X-ray source. Simultaneous thermogravimetric analysis−differential scanning calo-

https://dx.doi.org/10.1021/acsami.0c00196
ACS Appl. Mater. Interfaces XXXX, XXX, XXX−XXX

rimetry (TGA–DSC) measurements were performed with a TGA Q500, Thermal Analysis Instruments.

3. RESULTS AND DISCUSSION

The MTB electrolyte was synthesized by first dissolving 0.2 M of $Mg(CF_3SO_3)_2$ in DME and then adding 0.4 M of $MgCl_2$. After magnetic stirring for 6 h, 0.4 M $AlCl_3$ was slowly added to the above transparent solvent and stirred for 12 h at 60 °C. The resultant solution was clear and transparent (Figure S1), which remained clear and transparent eve after keeping for 2 months. To explore the optimum composition, we varied the contents of the Lewis acid $AlCl_3$ as shown in Figure S2. When the ratio of $MgCl_2/AlCl_3$ is 1:1, the electrolyte displays a higher current density and Coulombic efficiency of Mg^{2+} deposition/dissolution. Moreover, the effects of solvent on electrolyte were also investigated by varying the ether solvents. The Mg deposition/dissolution curves of MTB in DME, 2-methoxyethyl ether (G2), and tetraethylene glycol dimethyl ether (G4) are shown in Figure S3. A smaller polarization is observed when DME is used as a solvent compared with G2, and no obvious Mg deposition/dissolution behavior occurs in the G4 solvent. Therefore, the MTB electrolyte with DME solvent and an equal amount of $MgCl_2$ and $AlCl_3$ is an optimum choice. It was used in the following characterizations and electrochemical measurements.

Electrospray ionization-mass spectrometry (ESI-MS) was adopted to specify the equilibrium species of the MTB electrolyte. In the positive mode, the peak with a m/z ratio of 239.0 corresponds to $[Mg_2(\mu\text{-}Cl)_2(DME)_4]^{2+}$ (Figure 1a,b), which has been verified as an active cation that can enable reversible Mg deposition/dissolution.[29] $[Mg_2(\mu\text{-}Cl)_2(DME)_4]^{2+}$ contains two octahedrally coordinated Mg centers, two Cl atoms, and four DME ligands (Figure 1c). Two Mg centers are linked by two Cl atoms, while the other four coordinate sites of each Mg center are occupied by four oxygen atoms of two DME molecules. The counteranion is detected in a negative mode (Figure 1d). The peak with m/z of 282.8 is consistent with the simulated spectrum of $[(CF_3SO_3)AlCl_3]^-$ (Figure 1e). The molecular structure of this anion comprises a tetrahedrally coordinated Al center atom bridged with three Cl atoms and $CF_3SO_3^-$ ligand (Figure 1f). In the light of the previous reports,[30] the possible reaction in the MTB electrolyte is clarified in Figure 1g. When $Mg(CF_3SO_3)_2$ is dissolved in DME solvent, the solvated species are actually in the form of $[Mg(DME)_3]^{2+}$ (m/z of 147.0 in Figure 1a) and non-coordinating $CF_3SO_3^-$ (m/z of 148.9 in Figure 1d). Then, the acid–base reaction between the Lewis acid $AlCl_3$ and CF_3SO_3 yields a tetracoordinated $[AlCl_3(CF_3SO_3)]^-$ anion. One equivalent DME-solvated $MgCl_2$ further delivers one Cl^- to acceptor $[Mg(DME)_3]^{2+}$; as a result, two equivalent $[MgCl(DME)_2]^+$ cations are formed. Then, the pentacoordinated $[MgCl(DME)_2]^+$ cations convert to octahedrally coordinated $[Mg_2(\mu\text{-}Cl)_2(\kappa^2\text{-}DME)_4]^{2+}$ with better thermodynamic stability via a self-dimerization process.

The Mg deposition/dissolution behaviors in different cycles were characterized by cyclic voltammetry (CV) at 50 mV s^{-1} (Figure 2a). The first cycle shows no Mg deposition/dissolution behavior, and a small peak is observed after 30 cycles. Then, the peak current density of Mg deposition/dissolution increases in the next 20 cycles and gradually stabilizes. The corresponding Coulombic efficiency shown in Figure 2b is relatively low in the first 25 cycles, then sharply grows to 99.1%, and is maintained for 200 cycles. These results revealed that the MTB electrolyte

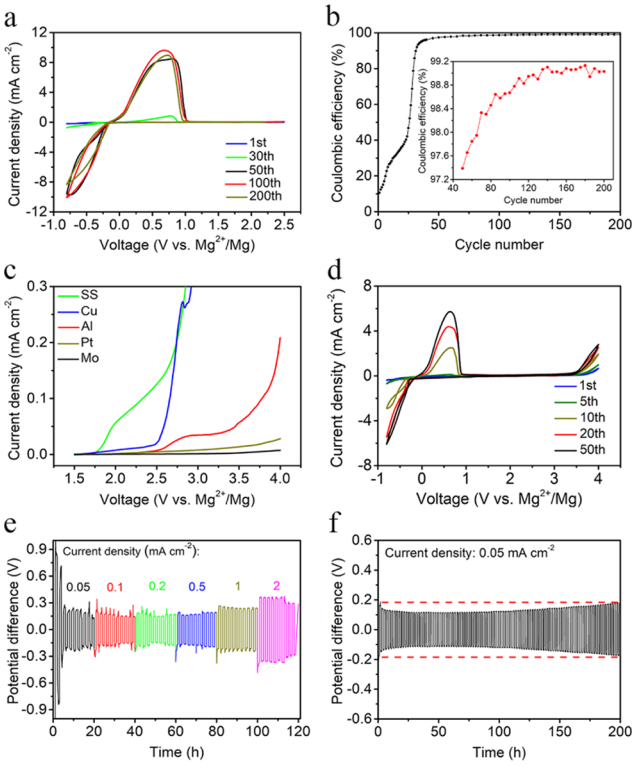

Figure 2. (a) CVs on Mo electrodes at 50 mV s^{-1} in a potential range of −0.8 to 2.5 V. (b) Corresponding Coulombic efficiency. Inset displays the Coulombic efficiency of 50–200 cycles. (c) LSVs on different metal electrodes. (d) CVs on Mo electrodes in a potential range of −1 to 4 V. (e) Polarization properties of Mg/Mg symmetrical cells with the MTB electrolyte at various current densities. (f) Long-term Mg deposition/dissolution in the MTB electrolyte at 0.05 mA cm^{-2}. The cycle time was 2 h per cycle (1 h discharging and 1 h charging).

undergoes an electrochemical conditioning process and then exhibits a superior deposition/dissolution performance after conditioning. Electrochemical oxidative stability is a crucial criterion for the properties of electrolytes. Linear sweep voltammetry (LSV) was tested at 1 mV s^{-1} to probe the stability of the MTB electrolyte with different current collectors, as shown in Figure 2c. The oxidative stabilities of the MTB electrolyte are ~3.5 and ~3.0 V when Mo and Pt are used as the working electrodes, respectively. However, it shows moderate oxidative stabilities against stainless steel (SS) (~1.75 V), Al (~2.5 V), and Cu (~2.5 V) current collectors due to the corrosion reaction between chlorides and non-noble metals. CVs on Mo electrode with a higher voltage window are tested in Figure 2d, verifying that the high oxidative stability of the MTB electrolyte is up to 3.5 V, which is consistent with the LSV result. Therefore, Mo foil is chosen to be the current collector in the following tests.

Symmetric Mg//MTB//Mg cells were assembled to evaluate the polarization characteristics of electrolyte. Figure 2e shows that the overpotential is only ~0.25 V at 0.05 mA cm^{-2} and reaches ~0.4 V when the current density is 2 mA cm^{-2}. As shown in Figure 2f, the overpotential is less than 0.25 V after 200 cycles at 0.05 mA cm^{-2}. The results signify the excellent stability and low polarization of the MTB electrolyte.

The Chevrel phase Mo_6S_8 is used for testing the compatibility of this MTB electrolyte for intercalation cathodes. Figure S4 shows the electrochemical properties of the Mg/Mo_6S_8 battery at 20 mA g^{-1}. The galvanostatic discharge/charge profiles

https://dx.doi.org/10.1021/acsami.0c00196
ACS Appl. Mater. Interfaces XXXX, XXX, XXX–XXX

(Figure S4a) display a defined plateau around 1.1 V with a low polarization of 0.1 V. After the conditioning process, the Mg/Mo_6S_8 battery keeps a stable specific capacity and high Coulombic efficiency (Figure S4b).

Further, this conditioning process is clarified to demonstrate the configurations of Mg_xCl_y species that react with sulfur and anions in the MTB electrolyte. The conditioning process is often present in the MACC electrolyte system. Previous studies have shown that the conditioning process may contribute to Mg and Al partial irreversible deposition, and the Mg/Al ratio finally reached an ideal stoichiometry.[26] Hence, the Mg/Al composition is explored at different conditioning states of the MTB electrolyte (Figure 3a and Table S2) by inductively coupled

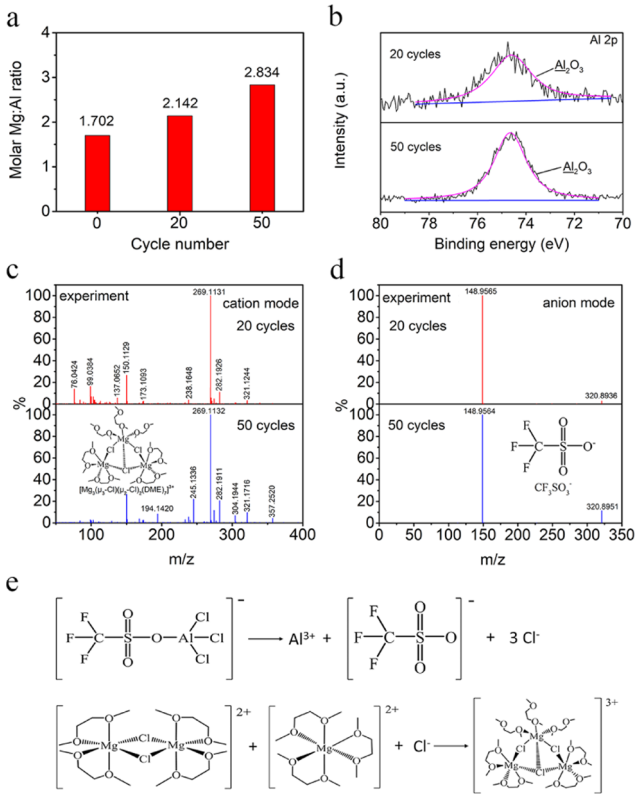

Figure 3. (a) ICP analysis of the molar Mg/Al ratio in the cycled MTB electrolyte. (b) Comparison of the surface XPS measurements of the Mg anode in the cycled MTB electrolyte. ESI-MS spectra of the cycled MTB electrolyte in (c) positive mode and (d) negative mode. (e) Possible reaction of the conditioning process in the MTB electrolyte.

plasma (ICP) analysis. The molar ratio of Mg/Al in the fresh electrolyte is 1.702 and then gradually rises to 2.834 after 50 cycles when the conditioning process is complete. Therefore, we speculate that in the initial stage of the conditioning process, Mg and Al were co-deposited. The content of Al gradually decreased due to the partially irreversible deposition of aluminum, so the Mg/Al ratio gradually increased with the conditioning process. To confirm this speculation, X-ray photoelectron spectroscopy (XPS) was carried out to reveal the surface evolution of Mg anodes cycled in the MTB electrolyte (Figure 3b). Both Al 2p spectra display that Al_2O_3 (~74.3 eV)[31] exists on the Mg surface and the intensity of the Al signal is increased as conditioning progresses. These results indicate that an irreversible Al deposition may occur on the Mg surface, which leads to an increase of Mg/Al ratio.[26] The decrease in Al^{3+} may change the ionic configurations in the electrolyte. ESI-MS was further conducted to identify this changing process in the MTB electrolyte. Figure 3c shows the spectra of the positive mode after 20 and 50 cycles. A primary m/z ratio of 269.1 could correspond to the simulated spectrum of $[Mg_3(\mu_3\text{-}Cl)(\mu_2\text{-}Cl)_2(DME)_7]^{3+}$ (Figure S5a). The anions transfer to $CF_3SO_3^-$ (m/z 148.9), as shown in Figures 3d and S4b. Based on the above results, the possible reaction during the conditioning process in the MTB electrolyte is proposed in Figure 3e. $[AlCl_3(CF_3SO_3)]^-$ is decomposed into Al^{3+}, Cl^-, and $CF_3SO_3^-$ during the deposition process of Al at the Mg surface. Then, free Cl^- and extra DME-solvated $[Mg(DME)_3]^{2+}$ are coordinated with $[Mg_2(\mu_2\text{-}Cl)_2(DME)_4]^{2+}$ to form the $[Mg_3(\mu_3\text{-}Cl)(\mu_2\text{-}Cl)_2(DME)_7]^{3+}$ cation.

To further explore the conditioning process of the electrolyte, ex situ Fourier transform infrared absorption spectrometer (FTIR) was performed. Figure S6 shows the FTIR spectra of the fresh MTB electrolyte and the electrolyte after 50 cycles. The peak at 840 cm^{-1} corresponded to the disappearance of the $(AlCl_3CF_3SO_3)^-$[25] anion after conditioning. Meanwhile, a new peak at 710 cm^{-1} corresponded to the appearance of $CF_3SO_3^-$. These results confirm the decomposition of the $(AlCl_3CF_3SO_3)^-$ anion after conditioning. The peak at 620 cm^{-1} is the vibrational peak of the Mg−Cl bond.[32] After conditioning, it shifts from 620 cm^{-1} to a higher wavenumber of 640 cm^{-1}, possibly due to the inductive effect caused by the increasing number of electron-withdrawing atoms Cl[33] in the conformation of $[Mg_3(\mu_3\text{-}Cl)(\mu_2\text{-}Cl)_2(DME)_7]^{3+}$ cation. The above results further demonstrate the reaction mechanism of the conditioning process (Figure 3e).

The deposition on the surface of the anode is directly related to the safety performance of the battery, so it is necessary to explore the morphology and composition of the deposition with XRD and SEM. The cell with Mo cathode and Mg anode was detached after consecutive CVs for 50 cycles at 50 mV s^{-1}. The XRD patterns (Figure 4a) and EDS spectrum (Figure 4b) confirm the co-deposition of Mg and Al on the surface of Mg foil, which is in accordance with the XPS results in Figure 3b. The SEM images are shown in Figure 4c,d, there is an obvious film without any dendrites observed on the Mg foil, indicating a uniform deposition. The XPS spectra were recorded to further analyze the surface chemical nature of the cycled Mg foil. There are two signals in the Mg 2p spectrum (Figure 4e): Mg^0 (~49.9 eV) and $MgCl_2$ (~51.2 eV).[31,34] The Cl 2p spectrum in Figure 4f shows that the split peaks of Cl $2p_{1/2}$ and Cl $2p_{3/2}$ at 199.7[35] and 198.5,[36] respectively, correspond to $MgCl_2$. The results of Figures 3 and 4 indicate that the surface of the Mg anode is uniformly deposited with Mg, Al, and $MgCl_2$, which further proves the speculation of the co-deposition of Mg and Al.

We assembled a cell based on vanadium nitrogen/sulfur (VN/S) cathode with Cu current collectors, Mg anode, and MTB electrolyte to verify the compatibility of the MTB electrolyte with a sulfur cathode. VN hollow nanospheres were chose as sulfur hosts because of several attractive properties:[37,38] (1) VN can effectively prevent the shuttle effect due to its highly efficient chemical absorption characteristic for polysulfides and (2) it has high electrical conductivity. The XRD pattern of the VN precursor (red line in Figure S7a) is consistent with that of pure crystalline VN phase (JCPDS No. 25-1252, space group: $Fm3m$). After the incorporation of sulfur into VN nanospheres, all of the diffraction peaks in the XRD pattern (blue line) correspond well with orthorhombic S (JCPDS No. 24-0733) and VN. The SEM and TEM images of VN/60S are displayed in

https://dx.doi.org/10.1021/acsami.0c00196
ACS Appl. Mater. Interfaces XXXX, XXX, XXX−XXX

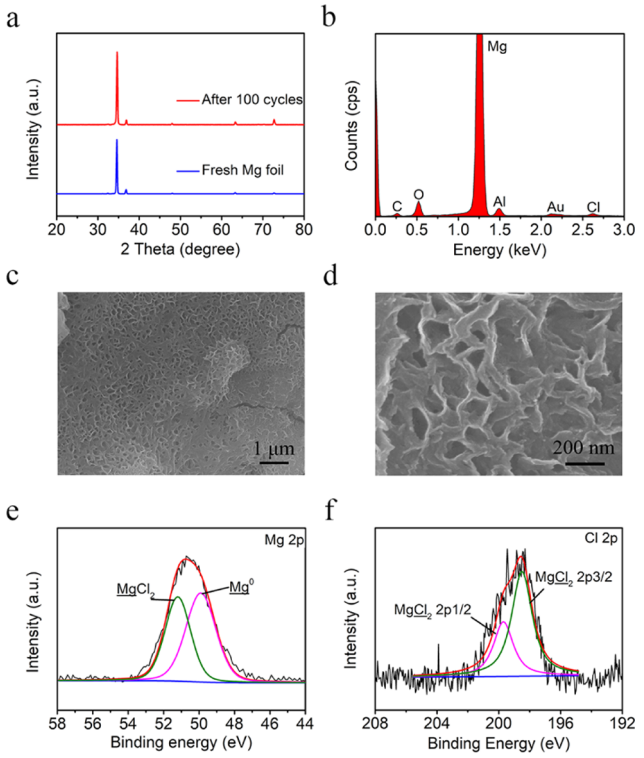

Figure 4. (a) XRD patterns and (b) EDS analysis of the Mg deposits. (c, d) SEM images of Mg deposits at different magnifications. XPS spectra recorded with Mg foil cycled for 50 times in the MTB electrolytes: (e) Mg 2p and (f) Cl 2p.

Figure S7b,c, which shows that VN/60S are composed of porous VN hollow spheres with an average diameter of ~200 nm and small sulfur particles on the surface and in the cavity of the VN spheres. The content of sulfur in the composites is 60 wt %, which is characterized by TGA−DSC under a Ar atmosphere in Figure S7d. The Cu current collectors have been verified to have no side reactions below 2 V (Figure S8).[11,39] Figures 5a and S9 show the galvanostatic discharge/charge profiles after the conditioning process at 200 mA g^{-1}. The discharge specific capacity is 812.7 mAh g^{-1} with a long plateau of ~1.1 V versus Mg, and the charge specific capacity is 808.1 mAh g^{-1} (based on the mass of sulfur). It shows a high Coulombic efficiency of 99.4%. The charge plateau is around ~1.68 V, resulting in low polarization of ~0.58 V. The corresponding cycling performance in Figure 5b shows the highest discharge capacity of 866 mAh g^{-1}, which remains at 844 mAh g^{-1} after 20 cycles. The capacity fluctuation in the 10th cycle may be due to the temperature fluctuation of the test environment.[40] The VN/60S also shows superior electrochemical performance at a higher current density of 500 mA g^{-1} (Figure 5c). The highest discharge specific capacity is 575 mAh g^{-1}, which remains at 450 mAh g^{-1} in the 100th cycle. It is worth noting that it exhibits a high power density of 550 W kg^{-1} (based on the mass of cathode active materials), which is the advanced level in the reported Mg/S batteries (Figure 5d).[4,8,12,13,16−18,24,41−46] The electrochemical properties of the obtainable Mg/S systems are summarized in Table S3. Our Mg/S system exhibits superior properties, especially in the charge−discharge overpotential and cyclic stability. Our work has promoted the development of high-power magnesium−sulfur batteries. Meanwhile, the low cost and facile preparation process further promote its practical application in Mg/S batteries. However, the conditioning process may limit its large-scale development in commercial applications. Further works on avoiding the conditioning process and improving the electrochemical performance are currently under investigation.

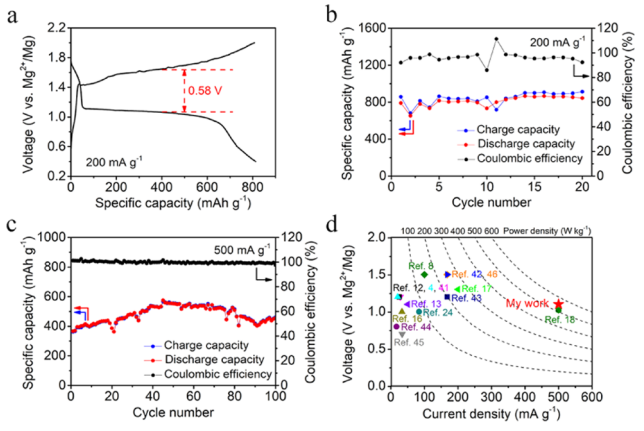

Figure 5. (a−c) Electrochemical characterization of the Mg-VN/60S battery after conditioning: (a) galvanostatic charge/discharge profile and (b) cycling performance at 200 mA g^{-1} and (c) cycling performance at 500 mA g^{-1}. (d) Comparison of power densities of Mg/S batteries.

4. CONCLUSIONS

A low-cost and non-nucleophilic $Mg(CF_3SO_3)_2$-based electrolyte for Mg/S battery was successfully designed. The active species in the MTB electrolyte composed of thermodynamically stable cations $[Mg_2(\mu\text{-}Cl)_2(DME)_4]^{2+}$ and tetracoordinated anions $[AlCl_3(CF_3SO_3)]^-$. This electrolyte displays a high Coulombic efficiency beyond 99.1% after the conditioning process, a relatively low overpotential less than 0.25 V, and high oxidative stability (~3.5 V). Particularly, the investigation of the conditioning process of this MTB electrolyte shows that the irreversible deposition of Al^{3+} leads to an ionic configuration transformation from $[Mg_2(\mu\text{-}Cl)_2(DME)_4]^{2+}$ to $[Mg_3(\mu_3\text{-}Cl)\text{-}(\mu_2\text{-}Cl)_2(DME)_7]^{3+}$. More importantly, the anion $CF_3SO_3^-$ greatly improves the compatibility of the electrolyte with the sulfur cathode, thereby effectively relieving the shuttle effect of the polysulfide and improving the kinetics. Therefore, a high specific capacity of 866 mAh g^{-1} at 200 mA g^{-1} and a high power density of 550 W kg^{-1} are obtained. Our work provides an effective way to develop low-cost and highly efficient electrolyte, which not only shows good compatibility with sulfur but can also be applied to general intercalation cathode materials, meaning that it promotes the development of Mg/S batteries and provides a new choice for RMBs.

■ ASSOCIATED CONTENT

Supporting Information

The Supporting Information is available free of charge at https://pubs.acs.org/doi/10.1021/acsami.0c00196.

Comparison of the costs of the electrolytes reported in the Mg/S battery system (Table S1); image of the prepared MTB electrolyte; electrolyte is clear and transparent, which remains clear and transparent after staying for two months (Figure S1); cyclic voltammogram of the Mo electrode in the MTB electrolyte with different $MgCl_2$/$AlCl_3$ ratios at 50 mV s^{-1} (Figure S2); CVs of the MTB

https://dx.doi.org/10.1021/acsami.0c00196
ACS Appl. Mater. Interfaces XXXX, XXX, XXX−XXX

electrolyte with different solvents at 50 mV s^{-1} (Figure S3); (a) Galvanostatic charge/discharge profiles and (b) cycling performance of the Mg/Mo_6S_8 battery at 20 mA g^{-1} (Figure S4); ICP analysis of the molar ratio of Mg/Al in the cycled MTB electrolyte (Table S2); simulated ESI-MS spectra of (a) $[Mg_3(\mu_3\text{-}Cl)(\mu_2\text{-}Cl)_2(DME)_7]^{3+}$ and (b) $CF_3SO_3^-$ (Figure S5); FTIR spectra of the pristine MTB electrolyte and the electrolyte cycled for 50 cycles (Figure S6); (a) XRD pattern, (b) SEM image, (c) TEM image, and (d) TG analysis of VN/60S (Figure S7); CVs of the Cu electrode in the MTB electrolyte at 50 mV s^{-1} (Figure S8); galvanostatic charge/discharge profile of the Mg-VN/60S battery after conditioning at a current density of 200 mA g^{-1} (Figure S9); comparison of the electrochemical performance for magnesium−sulfur batteries with previous reports (Table S3) (PDF)

AUTHOR INFORMATION

Corresponding Authors

Qinyou An − *State Key Laboratory of Advanced Technology for Materials Synthesis and Processing, International School of Materials Science and Engineering, Wuhan University of Technology, Wuhan 430070, Hubei, China*; Email: anqinyou86@whut.edu.cn

Liqiang Mai − *State Key Laboratory of Advanced Technology for Materials Synthesis and Processing, International School of Materials Science and Engineering, Wuhan University of Technology, Wuhan 430070, Hubei, China*; orcid.org/0000-0003-4259-7725; Email: mlq518@whut.edu.cn

Authors

Dan Huang − *State Key Laboratory of Advanced Technology for Materials Synthesis and Processing, International School of Materials Science and Engineering, Wuhan University of Technology, Wuhan 430070, Hubei, China*

Shuangshuang Tan − *State Key Laboratory of Advanced Technology for Materials Synthesis and Processing, International School of Materials Science and Engineering, Wuhan University of Technology, Wuhan 430070, Hubei, China*

Maosheng Li − *State Key Laboratory of Advanced Technology for Materials Synthesis and Processing, International School of Materials Science and Engineering, Wuhan University of Technology, Wuhan 430070, Hubei, China*

Dandan Wang − *Department of Materials Science and Engineering, University of Michigan, Ann Arbor, Michigan 48109, United States*

Chunhua Han − *State Key Laboratory of Advanced Technology for Materials Synthesis and Processing, International School of Materials Science and Engineering, Wuhan University of Technology, Wuhan 430070, Hubei, China*

Complete contact information is available at: https://pubs.acs.org/10.1021/acsami.0c00196

Author Contributions

[§]D.H. and S.T. contributed equally to this work.

Notes

The authors declare no competing financial interest.

ACKNOWLEDGMENTS

This work was supported by the National Natural Science Fund for Distinguished Young Scholars (51425204), the National Natural Science Foundation of China (51521001, 51972259, and 51602239), the National Key Research and Development Program of China (2016YFA0202603), the Programme of Introducing Talents of Discipline to Universities (B17034), and the Yellow Crane Talent (Science & Technology) Program of Wuhan City.

REFERENCES

(1) Zhou, L.; Zhang, K.; Hu, Z.; Tao, Z.; Mai, L.; Kang, Y.-M.; Chou, S.-L.; Chen, J. Recent Developments on and Prospects for Electrode Materials with Hierarchical Structures for Lithium-Ion Batteries. *Adv. Energy Mater.* **2017**, *8*, No. 1701415.

(2) Yoo, H. D.; Shterenberg, I.; Gofer, Y.; Gershinsky, G.; Pour, N.; Aurbach, D. Mg Rechargeable Batteries: An On-Going Challenge. *Energy Environ. Sci.* **2013**, *6*, 2265−2279.

(3) Xiong, F.; Fan, Y.; Tan, S.; Zhou, L.; Xu, Y.; Pei, C.; An, Q.; Mai, L. Magnesium Storage Performance and Mechanism of CuS Cathode. *Nano Energy* **2018**, *47*, 210−216.

(4) Zhao-Karger, Z.; Zhao, X.; Di, W.; Diemant, T.; Behm, R. J.; Fichtner, M. Performance Improvement of Magnesium Sulfur Batteries with Modified Non-Nucleophilic Electrolytes. *Adv. Energy Mater.* **2015**, *5*, No. 1401155.

(5) An, Q.; Li, Y.; Deog Yoo, H.; Chen, S.; Ru, Q.; Mai, L.; Yao, Y. Graphene Decorated Vanadium Oxide Nanowire Aerogel for Long-Cycle-Life Magnesium Battery Cathodes. *Nano Energy* **2015**, *18*, 265−272.

(6) Mao, M.; Gao, T.; Hou, S.; Wang, C. A Critical Review of Cathodes for Rechargeable Mg Batteries. *Chem. Soc. Rev.* **2018**, *47*, 8804−8841.

(7) Cui, L.; Zhou, L.; Zhang, K.; Xiong, F.; Tan, S.; Li, M.; An, Q.; Kang, Y.-M.; Mai, L. Salt-controlled Dissolution in Pigment Cathode for High-Capacity and Long-Life Magnesium Organic Batteries. *Nano Energy* **2019**, *65*, No. 103902.

(8) Gao, T.; Ji, X.; Hou, S.; Fan, X.; Li, X.; Yang, C.; Han, F.; Wang, F.; Jiang, J.; Xu, K.; Wang, C. Thermodynamics and Kinetics of Sulfur Cathode during Discharge in MgTFSI2-DME Electrolyte. *Adv. Mater.* **2018**, *30*, No. 1704313.

(9) Dai, C.; Lim, J. M.; Wang, M.; Hu, L.; Chen, Y.; Chen, Z.; Hao, C.; Bao, S. J.; Shen, B.; Yi, L.; Xu, M.; Henkelman, G. Honeycomb-Like Spherical Cathode Host Constructed from Hollow Metallic and Polar Co9S8 Tubules for Advanced Lithium-Sulfur Batteries. *Adv. Funct. Mater.* **2018**, No. 1704443.

(10) Dang, R.; Ma, X.; Liu, J.; Chen, M.; Zhang, Y.; Luo, J. Mesoporous MnO2 Fibers as an Efficient Bifunctional Absorber for High-Performance Lithium-Sulfur Batteries. *Int. J. Hydrogen Energy* **2018**, *43*, 18754−18758.

(11) Zhang, Z.; Dong, S.; Cui, Z.; Du, A.; Li, G.; Cui, G. Rechargeable Magnesium Batteries using Conversion-Type Cathodes: A Perspective and Minireview. *Small Methods* **2018**, *2*, No. 1800020.

(12) Nuli, Y.; Guo, Z.; Liu, H.; Yang, J. A New Class of Cathode Materials for Rechargeable Magnesium Batteries: Organosulfur Compounds Based on Sulfur−Sulfur Bonds. *Electrochem. Commun.* **2007**, *9*, 1913−1917.

(13) Zhang, Z.; Cui, Z.; Qiao, L.; Guan, J.; Xu, H.; Wang, X.; Hu, P.; Du, H.; Li, S.; Zhou, X.; Cui, G.; et al. Novel Design Concepts of Efficient Mg-Ion Electrolytes toward High-Performance Magnesium-Selenium and Magnesium-Sulfur Batteries. *Adv. Energy Mater.* **2017**, *7*, No. 1602055.

(14) Liebenow, C.; Yang, Z.; Lobitz, P. The Electrodeposition of Magnesium Using Solutions of Organomagnesium Halides, Amido-magnesium Halides and Magnesium Organoborates. *Electrochem. Commun.* **2000**, *2*, 641−645.

(15) Kim, H. S.; Arthur, T. S.; Allred, G. D.; Zajicek, J.; Newman, J. G.; Rodnyansky, A. G.; Oliver, A. E.; Boggess, W. C.; Muldoon, J. Structure and Compatibility of a Magnesium Electrolyte with a Cathode. *Nat. Commun.* **2011**, *2*, 427.

(16) Ha, S. Y.; Lee, Y. W.; Woo, S. W.; Koo, B.; Kim, J. S.; Cho, J.; Lee, K. T.; Choi, N. S. Magnesium(II) Bis(trifluoromethane sulfonyl) Imide-Based Electrolytes with Wide Electrochemical Windows for

Rechargeable Magnesium Batteries. *ACS Appl. Mater. Interfaces* **2014**, *6*, 4063−4073.
(17) Gao, T.; Hou, S.; Wang, F.; Ma, Z.; Li, X.; Xu, K.; Wang, C. Reversible S0/MgSx Redox Chemistry in MgTFSI2-MgCl2 Electrolyte for Rechargeable Mg/S Battery. *Angew. Chem., Int. Ed.* **2017**, *56*, 13526−13530.
(18) Du, A.; Zhang, Z.; Qu, H.; Cui, Z.; Cui, G.; et al. An Efficient Organic Magnesium Borate Based Electrolyte with Non-Nucleophilic Characteristic for Magnesium Sulfur Battery. *Energy Environ. Sci.* **2017**, *10*, 2616−2625.
(19) Deivanayagam, R.; Ingram, B. J.; Shahbazian-Yassar, R. Progress in Development of Electrolytes for Magnesium Batteries. *Energy Storage Mater.* **2019**, *21*, 136−153.
(20) Wu, N.; Yang, Z.; Yao, H.; Yin, Y.; Gu, L.; Guo, Y. Improving the Electrochemical Performance of the Li4Ti5O12 Electrode in a Rechargeable Magnesium Battery by Lithium-Magnesium Co-Intercalation. *Angew. Chem., Int. Ed.* **2015**, *54*, 5757−5761.
(21) Wang, W.; Liu, L.; Wang, P.; Zuo, T.; Yin, Y.; Wu, N.; Zhou, J.; Wei, Y.; Guo, Y. A Novel Bismuth-Based Anode Material with a Stable Alloying Process by the Space Confinement of an In Situ Conversion Reaction for a Rechargeable Magnesium Ion Battery. *Chem. Commun.* **2018**, *54*, 1714−1717.
(22) Pandey, G. P.; Hashmi, S. A. Experimental Investigations of an Ionic-Liquid-Based, Magnesium Ion Conducting, Polymer Gel Electrolyte. *J. Power Sources* **2009**, *187*, 627−634.
(23) NuLi, Y.; Yang, J.; Wu, R. Reversible Deposition and Dissolution of Magnesium from BMIMBF4 Ionic Liquid. *Electrochem. Commun.* **2005**, *7*, 1105−1110.
(24) Wang, P.; NuLi, Y.; Yang, J.; Feng, Z. Mixed Ionic Liquids as Electrolyte for Reversible Deposition and Dissolution of Magnesium. *Surf. Coat. Technol.* **2006**, *201*, 3783−3787.
(25) Yang, Y.; Wang, W.; Nuli, Y.; Yang, J.; Wang, J. High Active Magnesium Trifluoromethanesulfonate-Based Electrolytes for Magnesium−Sulfur Batteries. *ACS Appl. Mater. Interfaces* **2019**, *11*, 9062−9072.
(26) Barile, C. J.; Barile, E. C.; Zavadil, K. R.; Nuzzo, R. G.; Gewirth, A. A. Electrolytic Conditioning of a Magnesium Aluminum Chloride Complex for Reversible Magnesium Deposition. *J. Phys. Chem. C* **2014**, *118*, 27623−27630.
(27) Shao, Y.; Liu, T.; Li, G.; Gu, M.; Nie, Z.; Engelhard, M.; Xiao, J.; Lv, D.; Wang, C.; Zhang, J.-G.; Liu, J. Coordination Chemistry in Magnesium Battery Electrolytes: How Ligands Affect Their Performance. *Sci. Rep.* **2013**, *3*, No. 3130.
(28) Wu, C.; Zhang, X.; Ning, B.; Yang, J.; Xie, Y. Shape Evolution of New-Phased Lepidocrocite VOOH from Single-Shelled to Double-Shelled Hollow Nanospheres on the Basis of Programmed Reaction-Temperature Strategy. *Inorg. Chem.* **2009**, *48*, 6044−6054.
(29) He, S.; Luo, J.; Liu, T. L. MgCl2/AlCl3 Electrolytes for Reversible Mg Deposition/Stripping: Electrochemical Conditioning or Not? *J. Mater. Chem. A* **2017**, *5*, 12718−12722.
(30) Cheng, Y.; Stolley, R. M.; Han, K. S.; Shao, Y.; Arey, B. W.; Washton, N. M.; Mueller, K. T.; Helm, M. L.; Sprenkle, V. L.; Liu, J.; Li, G. Highly Active Electrolytes for Rechargeable Mg Batteries Based on a [Mg(μ-Cl)]2+ Cation Complex in Dimethoxyethane. *Phys. Chem. Chem. Phys.* **2015**, *17*, 13307−13314.
(31) He, Y.; Li, Q.; Yang, L.; Yang, C.; Xu, D. Electrochemical-Conditioning-Free and Water-Resistant Hybrid AlCl3/MgCl2/Mg(TFSI)2 Electrolytes for Rechargeable Magnesium Batteries. *Angew. Chem., Int. Ed.* **2019**, *58*, 7615−7619.
(32) Aurbach, D.; Turgeman, R.; Chusid, O.; Gofer, Y. Spectroelectrochemical Studies of Magnesium Deposition by In Situ FTIR Spectroscopy. *Electrochem. Commun.* **2001**, *3*, 252−261.
(33) Xin, H.; Wu, Q.; Han, M.; Wang, D.; Jin, Y. Alkylation of Benzene with 1-dodecene in Ionic Liquids [Rmim]+Al2Cl6X- (R= Butyl, Octyl and Dodecyl; X= Chlorine, Bromine and Iodine). *Appl. Catal., A* **2005**, *292*, 354−361.
(34) Fuggle, J. C.; Watson, L. M.; Fabian, D. J.; Affrossman. X-ray Excited Auger and Photoelectron Spectra of Magnesium, Some Alloys of Magnesium and Its Oxide. *J. Phys. F: Met. Phys.* **1975**, *5*, 375−383.
(35) Magni, E.; Somorjai, G. A. Electron-Irradiation-Induced Reduction of Magnesium-Chloride Thin-Films Deposited on Gold-Xps and Iss Study. *Surf. Sci.* **1995**, *341*, 1078−1084.
(36) Garbassi, F.; Pozzi, L. Electron Beam Effects on Hydrated Magnesium Chloride Revealed by XPS. *J. Electron Spectrosc. Relat. Phenom.* **1979**, *16*, 199−203.
(37) Ren, W.; Xu, L.; Zhu, L.; Wang, X.; Ma, X.; Wang, D. Cobalt-Doped Vanadium Nitride Yolk−Shell Nanospheres@Carbon with Physical and Chemical Synergistic Effects for Advanced Li−S Batteries. *ACS Appl. Mater. Interfaces* **2018**, *10*, 11642−11651.
(38) Sun, Z.; Zhang, J.; Yin, L.; Hu, G.; Fang, R.; Cheng, H. M.; Li, F. Conductive Porous Vanadium Nitride/Graphene Composite as Chemical Anchor of Polysulfides for Lithium-Sulfur Batteries. *Nat. Commun.* **2017**, *8*, No. 14627.
(39) Du, A.; Zhao, Y.; Zhang, Z.; Dong, S.; Cui, Z.; Tang, K.; Lu, C.; Han, P.; Zhou, X.; Cui, G. Selenium Sulfide Cathode with Copper Foam Interlayer for Promising Magnesium Electrochemistry. *Energy Storage Mater.* **2020**, *26*, 23−31.
(40) Luo, Y.; Xu, X.; Zhang, Y.; Pi, Y.; Zhao, Y.; Tian, X.; An, Q.; Wei, Q.; Mai, L. Hierarchical Carbon Decorated Li3V2(PO4)3 as a Bicontinuous Cathode with High-Rate Capability and Broad Temperature Adaptability. *Adv. Energy Mater.* **2014**, *4*, No. 1400107.
(41) Robba, A.; Vizintin, A.; Bitenc, J.; Mali, G.; Arčon, I.; Kavčič, M.; Žitnik, M.; Bučar, K.; Aquilanti, G.; Martineau-Corcos, C.; Randon-Vitanova, A.; Dominko, R. Mechanistic Study of Magnesium−Sulfur Batteries. *Chem. Mater.* **2017**, *29*, 9555−9564.
(42) Zhao-karger, Z.; Liu, R.; Dai, W.; Li, Z.; Diemant, T.; Vinayan, B. P.; Minella, C. B.; Yu, X.; Manthiram, A.; Behm, R. J.; Ruben, M.; Fichtner, M. Towards Highly Reversible Magnesium-Sulfur Batteries with Efficient and Practical Mg[B(hfip)4]2 Electrolyte. *ACS Energy Lett.* **2018**, *3*, 2005−2013.
(43) Yu, X.; Manthiram, A. Performance Enhancement and Mechanistic Studies of Magnesium-Sulfur (Mg-S) Cells with an Advanced Cathode Structure. *ACS Energy Lett.* **2016**, *1*, 431−437.
(44) Li, W.; Cheng, S.; Wang, J.; Qiu, Y.; Zheng, Z.; Lin, H.; Nanda, S.; Ma, Q.; Xu, Y.; Ye, F.; Zhang, Y.; et al. Synthesis, Crystal Structure, and Electrochemical Properties of a Simple Magnesium Electrolyte for Magnesium/Sulfur Batteries. *Angew. Chem.* **2016**, *128*, 6516−6520.
(45) Bevilacqua, S. C.; Pham, K. H.; See, K. A. Effect of the Electrolyte Solvent on Redox Processes in Mg−S Batteries. *Inorg. Chem.* **2019**, *58*, 10472−10482.
(46) Li, X.; Gao, T.; Han, F.; Ma, Z.; Fan, X.; Hou, S.; Eidson, N.; Li, W.; Wang, C. Reducing Mg Anode Overpotential via Ion Conductive Surface Layer Formation by Iodine Additive. *Adv. Energy Mater.* **2018**, *8*, No. 1701728.

https://dx.doi.org/10.1021/acsami.0c00196
ACS Appl. Mater. Interfaces XXXX, XXX, XXX−XXX